

S. Richter, G. Kukkadapu, C. K. Westbrook, M. Braun-Unkhoff, C. Naumann, M. Köhler, U. Riedel, A combined experimental and modeling study of combustion properties of an isoparaffinic alcohol-to-jet fuel, *Combustion and Flame* 240 (2022) 111994.

The original publication is available at www.elsevier.com

<https://doi.org/10.1016/j.combustflame.2022.111994/>

© <year>. This manuscript version is made available under the CC-BY-NC-ND 4.0 license <http://creativecommons.org/licenses/by-nc-nd/4.0/>

A combined experimental and modeling study of combustion properties of an isoparaffinic alcohol-to-jet fuel

Sandra Richter^{a*}, Goutham Kukkadapu^{b*}, Charles K. Westbrook^b, Marina Braun-Unkhoff^a,
Clemens Naumann^a, Markus Köhler^a, Uwe Riedel^{c,d}

^a German Aerospace Center (DLR), Institute of Combustion Technology,
Pfaffenwaldring 38-40, 70569 Stuttgart, Germany

^b Lawrence Livermore National Laboratory (LLNL), 7000 East Avenue, Livermore, CA 94551, USA

^c German Aerospace Center (DLR), Institute of Low-Carbon Industrial Processes,
Walther-Pauer-Straße 5, 03046 Cottbus, Germany

^d Stuttgart University, Institute of Combustion Technology for Aerospace Engineering,
Pfaffenwaldring 38-40, 70569 Stuttgart, Germany

***Corresponding authors:**

Sandra Richter

German Aerospace Center (DLR), Institute of Combustion Technology,
Pfaffenwaldring 38-40, 70569 Stuttgart, Germany
Sandra.Richter@dlr.de

Goutham Kukkadapu

Lawrence Livermore National Laboratory (LLNL),
7000 East Avenue, Livermore, CA 94551, USA
kukkadapu1@llnl.gov

This is a full-length article.

Shortened running title: Combustion properties of Alcohol-to-Jet SPK

Colored figures in online version only.

A combined experimental and modeling study of combustion properties of an isoparaffinic alcohol-to-jet fuel

Sandra Richter^{a*}, Goutham Kukkadapu^{b*}, Charles K. Westbrook^b, Marina Braun-Unkhoff^a,
Clemens Naumann^a, Markus Köhler^a, Uwe Riedel^{c,d}

^a German Aerospace Center (DLR), Institute of Combustion Technology, 70569 Stuttgart, Germany

^b Lawrence Livermore National Laboratory (LLNL), Livermore, CA 94551, USA

^c German Aerospace Center (DLR), Institute of Low-Carbon Industrial Processes, 03046 Cottbus, Germany

^d Stuttgart University, Institute of Combustion Technology for Aerospace Engineering, 70569 Stuttgart, Germany

* Corresponding authors: Sandra.Richter@dlr.de, kukkadapu1@llnl.gov

ABSTRACT

This work presents an investigation of fundamental combustion properties, specifically laminar burning velocity and ignition delay time, of an Alcohol-to-Jet Synthetic Paraffinic Kerosene (AtJ-SPK). Used in blends, this fuel is a sustainable aviation fuel that consists mostly of two long-chained, highly branched alkanes. Laminar burning velocities were measured at a preheat temperature of 473 K and pressures of 1 and 3 bar using the cone angle method. Ignition delay times of fuel-air mixtures diluted in nitrogen (N₂) were experimentally determined behind reflected shock waves at two fuel-air equivalence ratios, 1.0 and 2.0, at a pressure of 16 bar. In addition to these experiments, a modeling study was conducted using a new chemical kinetic reaction mechanism developed to describe the combustion behavior of the investigated AtJ-SPK. The simulations show that the new detailed mechanism is able to predict sufficiently the laminar flame speed at ambient pressure as well as the ignition delay time at elevated pressure. Sensitivity analyses for laminar flame speed and ignition delay time were performed as well.

Keywords: AtJ-SPK, alternative fuel, laminar flame speed, ignition delay time, reaction mechanism

1. INTRODUCTION

In 2019, the aviation industry accounted for about 2.1% of total anthropogenic carbon dioxide (CO₂) emissions, corresponding to a total amount of about 914 million tonnes CO₂ per year directly emitted into the upper atmosphere. Most (~80%) of these emissions result from long distance flights (over 1500 km) [1] for which no alternative of transport exists. Furthermore, the global aviation industry is a fast-growing sector, by about 2-3 percent per year, with no effect anticipated in the long-term perspective due to the corona pandemic. Thus, a respective cut in 2020/2021 is considered to be only a side effect – the emissions are expected to increase further as reported in earlier studies [2]. To address with this problem, technical improvements have been developed aiming at reducing fuel consumption and thus, of emissions, too; for example, achieving a higher bypass ratio defining the ratio between the mass flow rate of the bypass stream to the mass flow rate entering the core, by up to about 50-60, higher turbine inlet temperatures or the geared turbofan engine, besides others. To achieve a net CO₂ reduction in the near future, the only promising possibility is the development of sustainable aviation fuels (SAFs) being produced from renewable raw materials (biomass) or by employing the Power-to-Liquid (PtL) technology based on hydrogen by the use of (excess) renewable electricity, e.g. from wind power or photovoltaics, and a carbon source, such as carbon dioxide. Considering the renewable raw materials, lignocellulosic waste materials from agriculture and forestry are preferred, since they do not compete with food and forage production.

To date, seven different SAFs exist which are certified according to ASTM D7566 [3] for blending with conventional jet fuels Jet A and Jet A-1. One of these certified SAFs is the Alcohol-to-Jet Synthetic Paraffinic Kerosene (AtJ-SPK), developed and produced by Gevo, Inc., with the approval for blending with Jet A / Jet A-1 in amounts up to 50%. This specific renewable aviation fuel is produced from iso-butanol using a well-established fermentation process. AtJ-SPK consists mainly of two highly branched iso-alkanes: 2,2,4,6,6-pentamethyl heptane (i-C₁₂H₂₆, iso-dodecane) and 2,2,4,4,6,8,8-heptamethyl nonane (i-C₁₆H₃₄, iso-cetane) – the structures are shown in Fig. 1. Of the two iso-alkanes, iso-dodecane is present in relatively higher amounts of up to 83% by mole, while the

latter contributes to about 17% by mole. For all the simulations conducted in the present study and the validations shown in Supplementary Material (SM), this 83/17 molar composition has been used to represent the fuel.

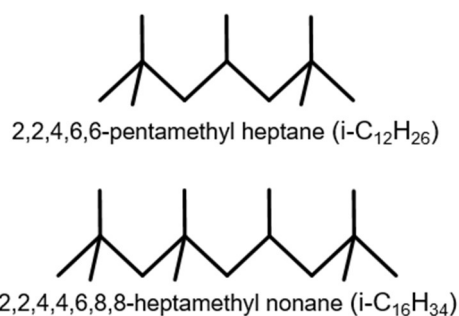


Figure 1 Molecular structure of the two dominant components of the considered Alcohol-to-Jet Synthetic Paraffinic Kerosene (AtJ-SPK).

The ignition characteristics of Gevo's AtJ-SPK have been studied, among others, by Guzman et al. [4] and Won et al. [5]. Guzman et al. [4] investigated both the oxidation and pyrolysis at temperatures between 900 K and 1550 K at $p = 4$ bar using a shock tube. Won et al. [5] studied the global oxidation characteristics of Gevo's AtJ-SPK, as well as other alternative fuels in a flow reactor at 12.5 atm within a temperature range of 500-1000 K. Further measurements of ignition delay times behind reflected shock waves were performed by Zhu et al. [6] in a temperature range from 1000 K to 1400 K for stoichiometric mixtures, and by Flora et al. [7] at temperatures between 980 K and 1800 K for fuel-lean mixtures. Measurements using a rapid compression machine (RCM) were done by Min et al. [8] and Valco et al. [9] at $625 \text{ K} < T < 725 \text{ K}$ and $p = 20$ bar. Recently, Wang et al. [10] proposed a physics-based model for simulating ignition characteristics of Gevo's AtJ-SPK, and validated their model against laminar flame speeds at $p = 1$ atm for unburned mixtures at 403 K, as well as ignition delay times at various conditions and speciation data obtained from shock tube and flow reactor facilities.

From literature review it is clear that the combustion behavior of Gevo's AtJ-SPK has not been studied comprehensively to allow a rigorous validation of chemical kinetic reaction models.

Understanding and enabling a more efficient and cleaner energy conversion is the driving force behind the current study with the focus set on providing laminar burning velocities at different pressures and shock tube ignition delay times of Gevo's AtJ-SPK at medium as well as high temperatures and at varying equivalence ratios. For comparison, the results for AtJ-SPK will be discussed with those of a crude-oil stemmed kerosene (Jet A-1) [11,12] measured using the same experimental conditions. The studied AtJ-SPK fuel as well as the Jet A-1 were both supplied by Bundeswehr Research Institute for Materials, Fuels and Lubricants (WIWeB) for a study on the sooting behavior of SAFs [12].

In addition to the experimental work, extensive chemical kinetic analysis using the new detailed model for AtJ-SPK is conducted.

2. EXPERIMENTS

2.1 Measurement of the laminar burning velocity

The laminar burning velocities (S_u) of the considered AtJ-SPK fuel were measured at a preheat temperature of $T = 473$ K, at pressures of $p = 1$ and $p = 3$ bar within a range of the fuel-air equivalence ratio (ϕ) between 0.6 and 1.5 by applying the cone angle method. An overview about the mixture composition and the parameter range for the measurement of the laminar burning velocity is given in Tab. 1.

Table 1 Mole fractions and oxidizer gas composition for the measurement of the laminar burning velocity (composition given in molar fraction for $\phi = 1.0$).

Mixture	Parameter range		
	Fuel-air ratio	Pressure	Temperature
AtJ-SPK + air (21% O ₂ + 79% N ₂)	0.60-1.50	1 bar	473 K
0.0106 AtJ-SPK + 0.2078 O ₂ + 0.7816 N ₂	0.70-1.45	3 bar	473 K

Since the method as well as the burner test rig have been used in previous studies of alternative aviation fuels [13,14], with experimental described in detail, only a short description of the experiment

is given here. A scheme of the experimental set up is presented in Fig. S1 within the Supplementary Material (SM). First, the fuel is vaporized at a temperature of ≈ 280 °C (≈ 550 K) for measurements at 1 bar and at $T = 320$ °C (≈ 590 K) for measurements at $p = 3$ bar, respectively. These high vaporization temperatures were selected reflecting the distillation curves of AtJ-SPK and Jet A-1, with the distillation curves' upper end being of about 250 °C (≈ 520 K) at $p = 1$ bar, and assumed to be 40 K higher at 3 bar. This allows to avoid fractionation of the components due to the different molecule sizes within the vaporizer. Directly after vaporization, the fuel is mixed with a preheated (temperature depends on the vaporization temperature) N₂-stream (Linde, 99.999%) and cooled down to the set temperature of $T = 473$ K to preclude a thermal decomposition of the fuel molecules. In a second mixing step, preheated (473 K) O₂ (Linde, 99.95%) is added yielding the specific fuel-air mixture. Since the retention time between the second homogenizer and the burner itself amounts only to about 0.5 s and 5 s (depending on the gas flow velocity). Thus, it is assumed that no fuel decomposition occurs even in the fuel-air mixture. Due to the sequential mixing with (i) N₂ and (ii) O₂ the partial pressure of the fuel is reduced resulting in the fuel's stabilization in the gaseous phase at 473 K, with no condensation occurring.

Premixed conical-shaped flames have been stabilized above a flame holder by the use of a co-flow, either air for rich flames ($\phi \geq 1.0$) or a mixture of 5% CH₄ + 5% H₂ + 90% N₂ for lean flames ($\phi \leq 1.0$). Stable flames are a prerequisite for the determination of burning velocity data using the cone angle (α) – see Fig. 2. Note that at fuel-rich conditions, the use of air as co-flow leads to the post-combustion of unburned hydrocarbons in the exhaust gas; for fuel-lean flames, the post-combustion of the excess oxygen is enabled with the CH₄/H₂/N₂-co-flow. Without post-combustion the range of fuel equivalence ratio for exploiting laminar burning velocity data is limited due to the occurrence of unstable flames caused by an increasing quenching distance to the nozzle. In both cases, the post-combustion process leads to a heat release in the exhaust gas which helps to stabilize the flame. This does not affect the measurements performed as checked always with an overlap of both specific co-flows around stoichiometric conditions. It was found that the burning velocities measured within this

overlap range were in accordance within the experimental uncertainties (for details regarding experimental uncertainties, see below and discussion in our previous work [13,14]).

The cone angle detection was performed by recording pictures with a CCD-camera (Imager Intense, LaVision). The laminar burning velocity (S_u) is calculated from the cone angle (α) of the flame and the gas velocity (v_u) of the unburned fuel-air mixture according to Eq. (1) [15,16] and Fig. 2. The gas velocity v_u is known from the volume flows of the gases (N_2 and O_2) controlled and measured using mass flow controllers (F-111B, Bronkhorst) as well as of the liquid fuel carried using a HPLC-pump (LC-20AD, Shimadzu). According to the fuel-air ratio, the volume flows were adjusted during the experiment. To cope with the issue of fluctuating cone angles resulting from changing flame lengths caused by flame instabilities and fluctuations, in particular at high fuel-air ratios, ten pictures were taken at each ϕ value and separately evaluated. For the determination of the laminar burning velocity, the average value was calculated.

$$S_u = v_u \cdot \sin\alpha \quad (1)$$

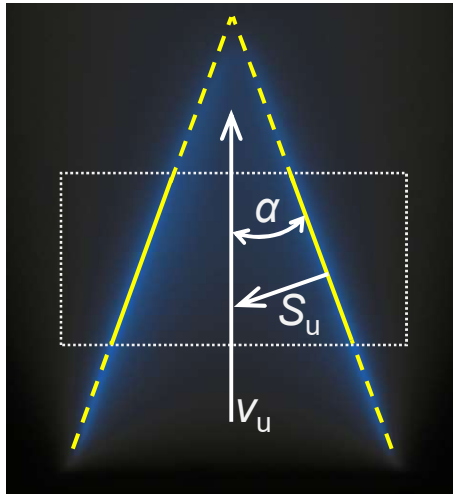


Figure 2 Relation between laminar burning velocity (S_u), cone angle (α), and flow velocity (v_u) of a laminar premixed conical flame.

The uncertainties of the laminar burning velocity reported herein correspond to the maximum error based on the error propagation. For the cone angle (α) the standard deviation from the evaluated pictures was determined and used as error whereas the error of the flow velocity (v_u) results from exactness of the total volume flow and of the nozzle diameter, the latter is limited to 0.005 mm. The precision of the volume flow is conditioned by the accuracy of the mass flow controllers and the experimental conditions, i.e. temperature and pressure having a deviation of ± 1 K and ± 5 mbar, respectively.

They are determined to be in a range between 2 cm/s and 5 cm/s with the highest values for fuel-rich mixtures and at elevated pressure resulting primarily from the determination of the cone angle due to difficulties during flame stabilization. Thus, the relative uncertainties amount to values between 3% and 6% for most of the experimental data with up to 10% for some single points. Further influence on the accuracy of the measurement arises from pressure and temperature variations as well as from the accuracy of the mass flow controllers. For more information, the reader is referred to our previous studies [13,14].

2.2 Measurement of ignition delay times

Ignition delay times were measured in a high-pressure shock tube (\varnothing 46 mm internal diameter), with a 10 m driver section and a 3.25 m driven section at an initial pressure of 16 bar for fuel-air mixtures with $\phi = 1.0$ and $\phi = 2.0$, respectively. The mole fractions of the fuel and the oxidizer gas composition for the experiments conducted in the present study have been provided in Tab. 2.

Table 2 Mole fractions and oxidizer gas composition for the measurement of the ignition delay (composition given in molar fraction), dilution 1:2 with N₂.

Mixture	Parameter range		
	Fuel-air ratio	Pressure	Temperature
AtJ-SPK + synthetic air (20% O ₂ + 80% N ₂)			
0.0051 AtJ-SPK + 0.0990 O ₂ + 0.8959 N ₂	1.00	16 bar	840-1710 K
0.0100 AtJ-SPK + 0.0980 O ₂ + 0.8920 N ₂	2.00	16 bar	900-1650 K

The experimental method was presented in detail previously (e.g., [13,17,18]) where the reader can find further information; additionally, a scheme of the experimental set up is presented in Fig. S2 as part of the Supplementary Material. Here, the driven section was heated to 433 K, the driver section to 393 K. He-Ar mixtures were used as driver gas to achieve tailored interface conditions [19]. Gas mixtures were prepared for each experiment by injecting the liquid fuel with a syringe onto fibers permanently purged by hot nitrogen; thus, evaporating and transporting the fuel into an evacuated mixing vessel. Preheated nitrogen and preheated synthetic air were added thereafter to adjust both the selected ϕ value and dilution d , here $d = 1:2$, diluted with nitrogen. Active mixing significantly reduced the time needed to achieve mixture homogeneity, thus preventing fuel degradation. Stable mixtures are assured by probing the mixture with GC/MS-measurements in a time series and determination of the recovery rates as well as the use of the one-mixture-one-shock approach: preparation of the mixture, filling the shock tube, loading and firing takes place within 15 minutes. Within this period of time and supported by the dilution with nitrogen, the determined fuel recovery rate is (95±5)%.

Ignition was identified by measuring the pressure profiles with piezo-electric gauges (PCB 112A22 and Kistler 603B coated with a thin layer of RTV116), located at a distance of 10 mm from the end plate. The chemiluminescence of excited CH-radicals (CH(A)) at 431 nm was detected axially via an end plate window (head-on) and radially (side-on) at distances of 10 mm, 70 mm, and 100mm away from the end plate simultaneously with the one of excited OH-radicals (OH(A)) at 308 nm amplified by logarithmic amplifiers (FEMTO HLVA-100). As a logarithmic amplifier maps (“compresses”) an input signal in a range of four decades to an output range of 0 to 1 V, thus being

very sensitive to low level signals; the decompression is done computationally using the characteristic of the amplifier to convert the output signal to the input. The benefit of the compression is the detection of very low-level emission signals such as from pre-ignition processes or for the detection of emission behind the incident shock front, indicating the upper temperature limit that can be achieved in the measurements without initiating reaction progress at the conditions behind the incident shock front.

Regarding the mixture stability behind the incident shock wave OH^{*}-, CH^{*}- and CO₂^{*}- emissions can be recorded applying a multispectral detection device at the end plate window. The signals are enhanced using a logarithmic amplifier. Thus, the dynamic range is highly enlarged for low signal detection. From the diaphragm's burst until the reflection of the incident shock front at the end plate, no chemiluminescence behind the incident shock front was observed that would indicate heat release or pre-ignition within the range of the experiments.

All ignition delay time values reported within the present work were determined by measuring the time difference between the initiation of the system by the reflected shock wave and the occurrence of the maximum of the CH(A)-emission signal at the measurement port located at a distance of 10 mm from the end flange (see Fig. 3). The initial temperature and pressure behind the reflected shock wave were computed from the incident shock speed, measured via four piezo-electric pressure gauges at intervals of 30 mm using a one-dimensional shock model. The estimated uncertainty in the initial reflected shock temperature is less than ± 15 K throughout the temperature range of our measurements. The relative error was derived from emission/absorption measurements in CO₂/Ar- and CO/Ar-mixtures by Roth [20] in this shock tube facility and reproduces the initial temperature calculated from the shock wave data within 1.5%. The error due to post-shock pressure increase has been quantified at 900 K using the reaction mechanism's predictions for a variation of the pressure of $\pm 20\%$. Here, the predicted deviation of the ignition delay time from the undisturbed pressure profile is between +6.2% at a pressure deviation of -20% to -11% at +20% for the equivalence ratios investigated.

Nevertheless, especially for longer ignition delay time measurements, post-shock compression due to the attenuation of the reflected shock interacting with the growing turbulent boundary layer

when propagating towards the contact surface (see pressure profile in Fig. 3), increases pressure and temperature of the mixture prior to heat release and ignition. This phenomenon was considered when modeling the (ignition) experiments by using an experimentally derived pressure profile provided to the modeling as $p = p(t)$ (see data file SM3 of the Supplementary Material).

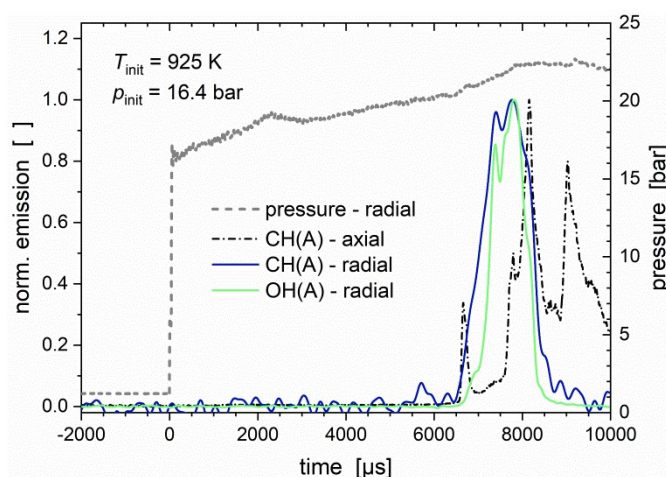


Figure 3 Measurement of ignition delay times: Typical pressure profile with post-shock compression, radially measured excited CH and OH radicals (CH(A) / OH(A)) as well as axially measured CH(A) emission profiles. Here, the emission is decompressed to the input signal of the logarithmic amplifier.

To avoid interference with pre-ignition heat release effects that superimpose on the post-shock pressure increase caused by gas dynamic effects, comparative measurements using non-ignitable gas mixtures of similar acoustic impedance, e.g. synthetic air / N_2 – mixtures without fuel, have been performed to support the derivation of this characteristic pressure profile. Shock tube measurements are considered to be closer to $p = p(t)$ than to $V = V(t)$ conditions, because pressure increase due to heat release takes effect not till then the heat release rate causing pressure increase is faster than the pressure relaxation towards the ‘open end’ of the reaction volume, i.e. towards the contact surface/driver section. Thus, the derived pressure profile used for the simulations is assumed to be suitable to trace the post-shock gas dynamics appropriately.

3. MODELING

3.1 Reaction mechanism for AtJ-SPK

While previous detailed chemical kinetic mechanisms have focused primarily on large n-alkane [21] and 2-methyl alkane [22] fuels as large as n-C₂₀H₄₂ and 2-methyl nonadecane, comparable kinetic models for highly branched alkane fuels have been limited almost exclusively to iso-octane, with only a few modeling studies on larger iso-alkanes. However, current interests have begun to address larger branched fuels, which often have benefits including much better resistance to autoignition and engine knock, and possibly reduced soot production. A very recent study [4] included the components in the present AtJ-SPK fuel, together with iso-nonane (2,2,3,3-tetramethyl pentane) and iso-tridecane (2,6,8-trimethyl decane), which were investigated in a combined experimental and modeling study where a single pulse shock tube was used for the measurements. Comparisons between experiments and modeling results were used to partially validate the high temperature kinetic mechanisms for iso-dodecane and iso-cetane. Building on the mechanism from Guzman et al. [4], an updated iso-alkane model which includes the low temperature kinetics of iso-dodecane was recently developed at LLNL and presented in Fang et al. [23]. The detailed kinetic model of Oehlschlaeger et al. [24] is one of the few detailed kinetic models available for iso-cetane. The improvements suggested in the recent work of Kukkadapu et al. [25] were needed for the iso-cetane mechanism of Oehlschlaeger et al., particularly for the low temperature chemistry. Also, recent works [26-28] from LLNL, NUIG, and KAUST have demonstrated the need for updating the thermochemistry of the low temperature chemistry related species, updating the reaction rates for various reaction classes and finally, the need for addition of so-called “alternative isomerization pathways” of O₂QOOH species (see below).

Recognizing the need for an updated kinetic model for iso-cetane, several changes were made to the earlier mechanism of Oehlschlaeger et al. [24], which include 1) using the improved C₀-C₄ AramcoMech 2.0 [29] base mechanism, 2) adopting the C₅-C₁₂ mechanism from Fang et al. [23], 3) re-evaluating the thermochemistry of the intermediate species using the group additivity approach of Benson using the latest group values from Burke et al. [30], and 4) addition of alternative reactions of

O₂QOOH species, and modifying the reactions rates of several reaction classes. To our knowledge, experimental or ab-initio studies aimed at assessing the rate parameters of the various plausible reactions of iso-dodecane and iso-cetane are not available in literature. Hence, we rely on the principles of reaction analogies and associated rate parameters to model the kinetics for building the kinetic model for Gevo-fuel surrogates. The references to the reaction rate rules, reaction classes updated are provided in Tab. 3. Also, the rate rules and analogies adopted in the mechanism have been adopted from recent LLNL, NUIG, and KAUST [26-28] mechanism on C₅-C₁₂ paraffins to ensure to near consistency and shall be briefly discussed here in.

The reaction rates for the high temperature reaction classes 1-9 (as described by Curran et al. [31,32]) have largely been taken from the earlier work of Mehl et al. [33] with an exception of H abstraction by OH which were taken from the work of Badra and Farooq [34]. The rate parameters used for H-abstractions are site specific and in the case of abstractions by OH are also dependent on the next-nearest-neighbor (N-N-N) carbon atoms. Among the low temperature reactions classes, we have updated the rates of reactions classes #10, #12, #17, #19-25, which pertain to low-temperature peroxy chemistry using the rate parameters from ab-initio studies of Sharma et al. [35], Villano et al. [36,37], and Miyoshi [38]. In addition to the 25 classes earlier described in Curran et al. [31,32], the reaction classes corresponding to concerted elimination of alkyl peroxy radicals (commonly referred as RO₂ radicals) and hydroperoxyl alkylhydroperoxides (commonly referred as O₂QOOH radicals), and the alternative isomerization reactions of O₂QOOH radicals producing the dihydroperoxy alkyl radicals (P(OOH)₂), which Sharma et al. [35] proposed have also been added. The rates for these reaction classes have been taken from Villano et al. [36]. For the alternative reactions of O₂QOOH radicals, current model includes the alternative isomerization reactions of all O₂QOOH radicals. The (P(OOH)₂) radicals have been modelled to be consumed by reactions producing the hydroperoxyl cyclic ether (HPCE) which are analogous to the formation of cyclic ethers from alkyl hydroperoxy radicals (commonly referred as QOOH).

Table 3 List of reaction classes and the references for the rate rules used based on analogy.

Class	Description of reaction type	Reference	Site specific rate rule (p/s/t)
#1	Unimolecular fuel decomposition	[33]	Yes
#2	H-abstractions from the fuel by $\dot{O}H$, \dot{H} , \dot{O} , and $\dot{C}H_3$	[33,34]	Yes
#3	Fuel Radical decomposition	[33]	Yes
#4	$R+O_2=$ olefin+ HO_2	[33]	Yes
#5	Fuel Radical isomerizations	[33]	Yes
#6	Abstraction reactions from olefin by $\dot{O}H$, \dot{H} , \dot{O} , and $\dot{C}H_3$	[33]	Yes
#7	Addition of radical species to olefin	[33]	Yes
#8	Alkenyl radical decomposition	[33]	Yes
#9	Unimolecular Olefin decomposition	[33]	Yes
#10	O_2 addition to fuel radicals, $R+O_2=RO_2$	[38]	Yes
#11	$\dot{R} + R'\dot{O}_2 = R\dot{O} + R'\dot{O}$	[33]	No
#12	Alkyl peroxy radical isomerization ($R\dot{O}_2 \rightleftharpoons \dot{Q}OOH$)	[36]	Yes
#13	$R\dot{O}_2 + H\dot{O}_2 = RO_2H + O_2$	[33]	No
#14	$R\dot{O}_2 + H_2O_2 = RO_2H + H\dot{O}_2$	[33]	No
#15	$R\dot{O}_2 + CH_3\dot{O}_2 = R\dot{O} + CH_3\dot{O} + O_2$	[33]	No
#16	$R\dot{O}_2 + R'\dot{O}_2 = R\dot{O} + R'\dot{O} + O_2$	[33]	No
#17	$RO_2H = R\dot{O} + \dot{O}H$	Estimate (see text)	No
#18	$R\dot{O}$ decomposition	[33]	No
#19	$\dot{Q}OOH =$ Cyclic ether + $\dot{O}H$	[38]	Yes
#20	$\dot{Q}OOH =$ olefin + $H\dot{O}_2$	[37]	Yes
#21	$\dot{Q}OOH$ decompositions	[37]	Yes
#22	Addition of $\dot{Q}OOH$ to O_2	[38]	Yes
#23	$O_2\dot{Q}OOH=$ KHP+ OH	[35]	Yes
#24	Decomposition of ketohydroperoxide	Estimate (see text)	No
#25	Cyclic ether reactions with $\dot{O}H$ and $H\dot{O}_2$	Estimate	No
New	$RO_2=HO_2+OLEFIN$	[36]	Yes
New	$O_2\dot{Q}OOH= P(OOH)_2$	[36]	Yes
New	$P(OOH)_2= HPCE+OH$	[38]	Yes
New	HPCE decomposition	Estimate (see text)	No

For the decomposition reaction of hydroperoxides (ROOH, KHP and HPCE) we used rate parameters: ($1e16 \text{ s}^{-1}$, 0, 42.3 kcal/mole) which are close to the geometric mean of the rate available for decomposition of hydroperoxides [39,40]. The rate parameters for consumption reaction of cyclic ethers by OH and HO₂ radicals have been re-estimated using the method as suggested in the earlier work of Curran et al. [31,32] but using the latest rates for abstraction by OH and HO₂. The primary function of the additional low temperature reaction pathways is to revise the details of the chain branching, chain propagation, and chain termination functions in the kinetic mechanism.

This mechanism consisting of 1832 species and 7337 reactions now available to simulate Gevo-fuel chemistry was checked against the LLNL cloud tool [41] to identify reactions which violate collisional limit, bad thermochemistry and species which are chemical dead ends and the report has been attached with the supplementary material. As seen in the report, we still have reactions which violate the collisional limit especially at very low temperatures (around 300 K), but this is due to lack of better characterization of the rate parameters at these very low temperatures. Resolving this would need better characterization of the rates using ab-initio studies, and beyond the scope of the present study. The kinetic mechanism, thermochemistry database, and transport data files are included in the Supplementary Material and will also be available via the LLNL website.

3.2 Calculation of laminar flame speed

Laminar flame speeds have been computed using the LLNL's transient laminar flame speed module [42] on zero-RK solvers [43] while the sensitivity analyses were conducted using Chemkin-Pro [44].

3.3 Calculation of ignition delay time

For simulations of the experiments with detailed chemical kinetic reaction mechanisms, an adaption of the SENKIN code of the CHEMKIN II program suite was used [45,46]. Ignition delay times were defined as the time of maximum CH(A) concentration accordingly applied to the

experiments. To estimate the variance of ignition delay time calculations imposed by the pressure profile computations were performed at a temperature of 900 K for $p = p(t/s > 0) \pm 20\%$. The result for each considered ϕ value is provided in Fig. 7 (section 4.2) as error bar to the computed ignition delay time profile. The impact of the pressure profile can describe as follows; a figure is given in the supplementary material (Fig. S6).

(i) The pressure profile used in the chemical kinetic calculations is derived from pressure profiles measured in the lower Mach number range of our series and without the influence of heat release due to the ignition process. This process has been verified by using a mixture unable to release heat at the experimental conditions, but emulating the acoustic behavior (usually done by substituting O₂ by CO or at this very low initial fuel concentrations simply by using a SynAir/N₂-mixture).

(ii) In the calculations, the pressure increase will be treated by the energy equation providing the pressure profile derived from (i), increasing temperature like an adiabatic isentropic compression. Additionally, the released heat will attribute to a further temperature increase, but this is not translated into pressure increase for the following reason: Because the reaction volume is open towards the driver section, pressure increase will only take place, if the heat release rate becomes larger than the pressure relaxation. This effect cannot be handled in a 0-dim. model. This was investigated with a so called “Multiple Plug Flow Reactor” model (MPFR-model) [47]. In this model, the shock tube is distributed into slices (0-dim. reactors) that are initialized by the reflected shock front according to its propagation velocity and acoustically coupled in direction of the axis (quasi 1-dim). The heat release was translated into pressure increase, that could propagate towards the closed and the open end of the tube. Eventually, the pressure of the initial PFR closest to the end plate was calculated as superposition of all pressure relaxation events in the reactor slice. The effect on ignition delay time was not significant, except only for very short times before ignition.

(iii) The impact of the pressure profile is demonstrated using the pressure profile derived from the experimental investigations in (i) but varying the increase by $\pm 20\%$ for $t/s > 0$. Thus, the effect of adiabatic isentropic compression as described in (ii) will be stronger or weaker and the ignition delay

times calculated will be shorter or longer. This provides a figure to quantify the impact of the pressure profile derived from the experiments.

Brute force sensitivity analyses for 0-D ignition delays were also conducted using zero-RK solvers [39]. In this analysis, a reference ignition delay time $\tau_{\text{ign}}(k_i)$ is computed for a kinetic problem using a full, given set k_i of i reactions. The same problem is then computed again, using exactly the same model, except that a selected individual reaction rate has been multiplied by a factor ' f ', producing a new result for the ignition delay time $\tau_{\text{ign}}(f \cdot k_i)$ that can be compared with the ignition delay time computed using the reference kinetic mechanism. The ignition delay time sensitivity coefficient (S_i) for that reaction " i " is then computed according to Eq. (2) as

$$S_i = \ln (\tau_{\text{ign}}(f \cdot k_i) / \tau_{\text{ign}}(k_i)) / \ln(f) \quad (2)$$

Based on this definition, reactions which accelerate ignition exhibit negative values and the reactions that retard ignition exhibit positive sensitivity coefficients. For this sensitivity analysis, a common CHEMKIN approach – the time of attaining the initial temperature plus 400 K – was chosen. This definition was used for ignition delay instead of maxima in maximum CH(A) concentration as it reduces the computational time, and the controlling chemistry is expected not to change with either of the choices for identifying ignition delay.

4. RESULTS AND DISCUSSION

4.1 Laminar burning velocity

Figure 4 (top) shows the comparison of the measured laminar burning velocities of AtJ-SPK from the present study along with data of Jet A-1 fuel and the literature data of iso-octane [48] measured using the same experimental set up at varying pressures and an initial pre-heat of 473 K. The comparison of the burning velocities shown in Fig. 4 helps understand the dependence of the laminar burning velocities on pressure and also the effect of composition and structure of the hydrocarbon

fuels. Regarding the former, the burning velocity decreases with increase in pressure. Also, from the current measurements, the maxima of the burning velocity of AtJ-SPK are located at $\phi = 1.05$ with 78.4 cm/s for $p = 1$ bar and at $\phi = 1.10$ with 63.3 cm/s for $p = 3$ bar, respectively.

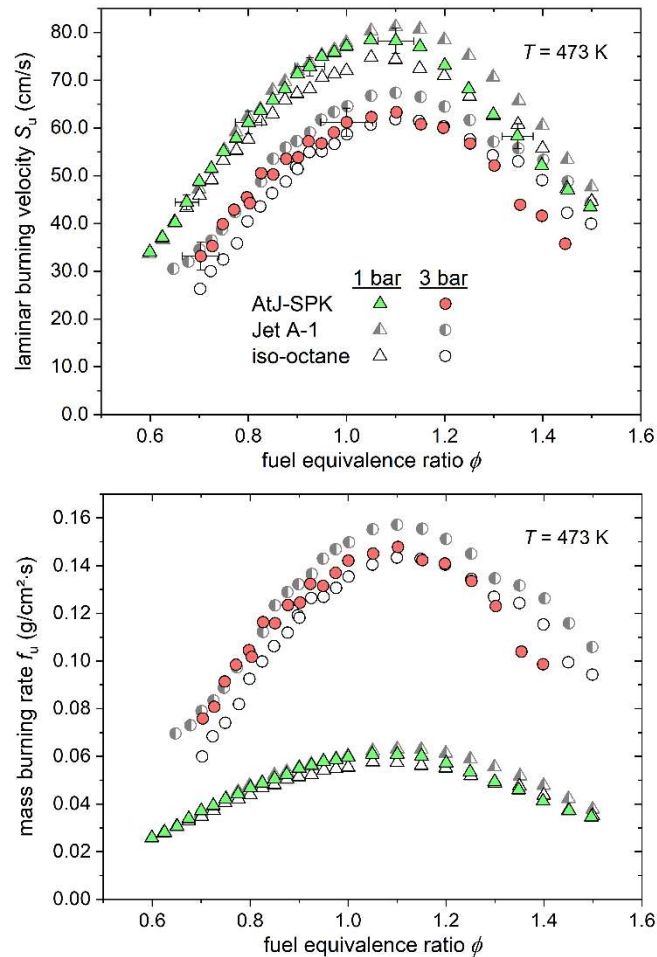


Figure 4 Results of the measured laminar burning velocities (top) and mass burning rate (bottom) of fuel/air mixtures for AtJ-SPK (Alcohol-to-Jet Synthetic Paraffinic Kerosene) in comparison with experimental data of Jet A-1 [11,12] and iso-octane [48] measured at the same experimental conditions.

From Fig. 4 it can be noticed that the burning velocities of AtJ-SPK and iso-octane peak values – $S_u = 74.8$ cm/s at $p = 1$ bar ($\phi = 1.05$), $S_u = 61.8$ cm/s at $p = 3$ bar ($\phi = 1.10$) – are closer to each other than the ones of AtJ-SPK and Jet A-1. For fuel-lean mixtures, the results obtained for Jet A-1 and AtJ-

SPK were even closer together whereas iso-octane shows significantly lower values. However, AtJ-SPK and iso-octane show similar LBV values with a larger difference to Jet A-1, at 1 bar with $\phi > 1.15$ as well as at 3 bar between $\phi = 0.90$ and $\phi = 1.30$. Moreover, AtJ-SPK and iso-octane yield a general trend to lower LBV values compared to Jet A-1. This can be attributed to the underlying similarities in the functional group makeup of both the fuels. Both AtJ-SPK and iso-octane are C₄ iso-alkane oligomers [49], and at high temperatures both the fuels break down into the iso-butane (tert-butyl radical, iso-butene, iso-butenyl radicals) derivatives; hence, resulting in the similarity in the laminar burning velocities.

The comparison of the experimental results at 473 K for AtJ-SPK to the measurements of Jet A-1, shown in Fig. 4 as well, yields a trend to higher values of the conventional fuel (Jet A-1), especially for stoichiometric and fuel-rich mixtures, by up to about 2 cm/s difference at $\phi = 1.05$ and a maximum difference of 8 cm/s between $\phi = 1.25$ and $\phi = 1.45$. Since it is well known that branched fuel molecules lead to lower burning velocities compared to fuels consisting predominantly of linear molecules, this difference results from the highly branched structure of the AtJ-SPK fuel molecules (due to the occurrence of the tert-butyl radical during the oxidation process) being ‘unusual’ for liquid jet fuels. Usually, a jet fuel contains predominantly straight n-alkanes, and only slightly branched iso-alkanes, besides cyclic and aromatic components [50].

In addition to the laminar burning velocity S_u also the mass burning rate f_u was determined according to Eq. (3) [51] using the density of the unburned gas mixture ρ_u . The higher mass burning rate shown in Fig. 4 (bottom) at 3 bar corresponds to the higher gas density. Regarding the comparison of the considered fuels, this evaluation yields the same trend as shown for the laminar burning velocity with lower values of the mass burning rate for AtJ-SPK and iso-octane than for Jet A-1.

$$f_u = \rho_u \cdot S_u \quad (3)$$

Comparison of the flame speeds of AtJ-SPK (this work) as well as of iso-octane [48] obtained from measurements (symbols) and those obtained from predictions using the new LLNL mechanism (curves) is shown in Fig. 5. The performance of the new LLNL model is satisfying at atmospheric pressures: Between $\phi = 0.6$ and $\phi = 1.3$ the experimental data of iso-octane are perfectly matched by the calculations whereas the data of AtJ-SPK are slightly underpredicted by about 4 cm/s corresponding to a deviation of 5% (at $\phi = 1.05$). Only for $\phi > 1.30$ the modeling yields an underprediction of the experiment for both fuels. At elevated pressure (3 bar), the performance of the mechanism is quite similar for AtJ-SPK and iso-octane: The differences between measurements and LLNL mechanism predictions are small at fuel-lean conditions but increase with increasing fuel equivalence ratio resulting in an underprediction of the flame speeds by up to about 20% at fuel-rich condition.

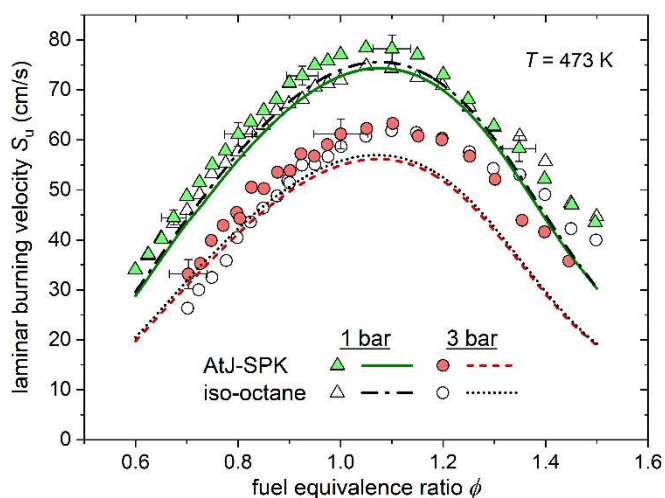


Figure 5 Results of the measured (symbols) laminar burning velocities for AtJ-SPK (Alcohol-to-Jet Synthetic Paraffinic Kerosene) and iso-octane [48], each in mixture with air at $T = 473$ K in comparison with calculated flame speeds (curves) using the new LLNL mechanism (present work).

In order to describe further the accuracy of the mechanism the error function approach as suggested from Olm et al. [52] is used. The error function value describes the deviation between simulation and experiment with respect to the experimental uncertainty. If the difference between simulation and

experiment is similar to the experimental uncertainty, the error function value is close to unity. In Fig. 6 the estimated error function values and average deviations are compared for each fuel and pressure. As already shown, this evaluation yields higher values for 3 bar than for 1 bar regarding the error function as well as the average deviation. Considering the accuracy of the simulation for each fuel, a higher average deviation for AtJ-SPK than for iso-octane is obtained whereas the resulted error function value for AtJ-SPK is lower. Here, the influence of the experimental uncertainty becomes noticeable being slightly higher for AtJ-SPK compared to iso-octane.

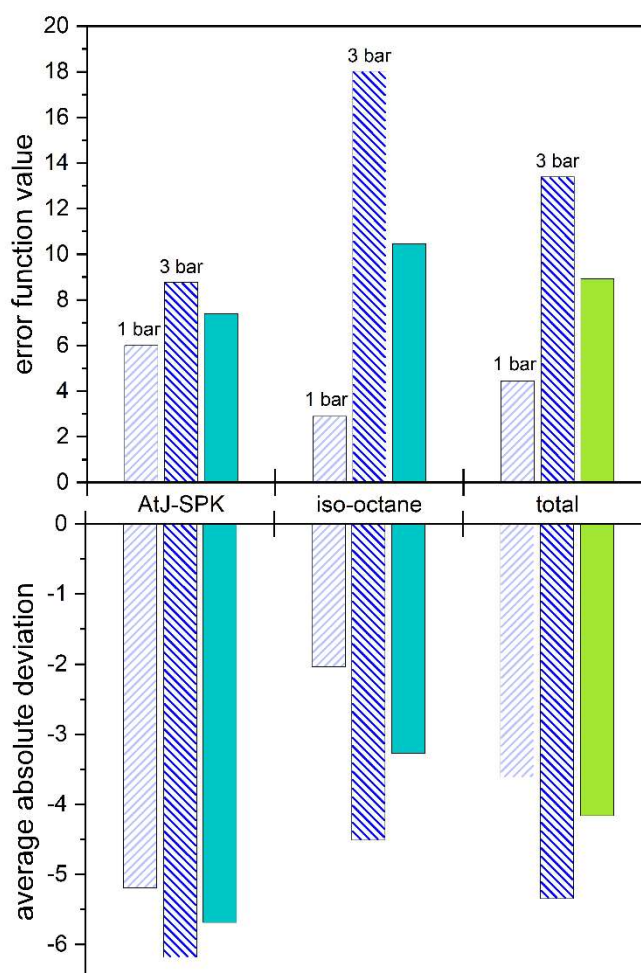


Figure 6 Evaluation of the accuracy of the mechanism using the error function value and the average absolute deviation as described by Olm et al. [52].

The comparison of the flame speeds at $p = 3$ bar illustrates the challenges associated with (i) the measurement of rich fuel-air mixtures at elevated pressures, and (ii) modeling the combustion characteristics of severely branched fuels and the need of data for the validation of chemical kinetic mechanisms. In the range of the maximum the flames speed is underpredicted by about 4 cm/s resulting in a difference between measured and calculated data of less than 10% being in the maximum uncertainty found in the experiment. Since the mechanism shows – even at fuel-rich conditions – reasonable results at 1 bar, the larger deviations at 3 bar and at fuel-rich conditions are explained by the challenging realization of a stable flame at higher pressures and high fuel-air ratios (see section 2.1).

A comparison of the predicted laminar flame speed of AtJ-SPK at 403 K using the LLNL mechanism from the present work to experimental data from Wang et al. [10] is given in Fig. S3 of the supplementary material. With only a slight overprediction the new mechanism reproduces these experimental data as well.

To get a deeper insight into the reaction network, sensitivity analyses were performed for AtJ-SPK at $\phi = 1.0$ for $p = 1$ bar and $p = 3$ bar by using the new LLNL model as developed within the present work – the results are shown in Fig. 7. Overall, the sensitivities are very similar for both pressures considered, with the chain branching reaction $\text{O}_2 + \text{H} \Leftrightarrow \text{O} + \text{OH}$ as identified as the most sensitive reaction, followed by further reactions generating H atoms as well as H/CO reactions. Most of these reactions show a slightly higher sensitivity at $p = 3$ bar being caused by the higher particle (fuel) density.

In these analyses, the computed AtJ-SPK flame speeds are not observed to be sensitive to fuel specific reactions (at least among the first 13 most sensitive reactions); the flame speed predictions are controlled by the base C₀-C₄ reaction network for the current fuels. From this, the differences in predicted flame speeds are inferred to be not necessarily due to the sub-models of the parent fuels (here: 2,2,4,6,6-pentamethyl heptane (i-C₁₂H₂₆, iso-dodecane) and 2,2,4,4,6,8,8-heptamethyl nonane (i-C₁₆H₃₄, iso-cetane)); the differences could be due to uncertainties in experiments, or due to the

simplicity of the surrogate used for modeling the ‘real’ AtJ-SPK or due to potential discrepancies in the C₀-C₃ sub-model partly taken from the AramcoMech 2.0 [29].

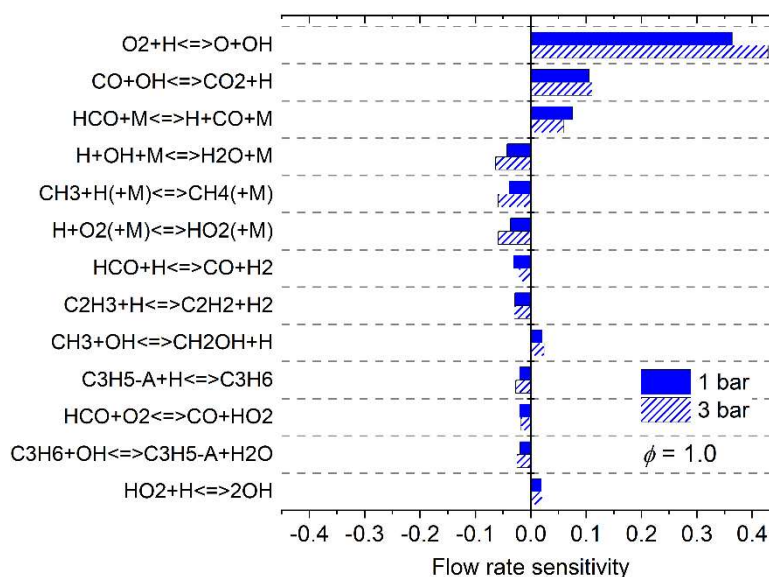


Figure 7 Sensitivity analysis of laminar flame speed of AtJ-SPK at fuel-air equivalence ratio $\phi = 1.0$.

4.2 Ignition delay time

The results of the measured ignition delay time data as well as the calculated ones by using the newly developed LLNL mechanism (this work) are presented in Fig. 8. The ignition delay time data as measured at the two fuel-air ratios ($\phi = 1$ and $\phi = 2$) are very close to each other within the accessible temperature range, from 830 K to 1670 K. In detail, at $T < 1000$ K the stoichiometric mixture has longer ignition delay times than the fuel-rich mixture whereas at $T > 1500$ K ignition delay time data of the stoichiometric mixture are slightly shorter. These differences are more pronounced concerning the ignition delay time data predicted using the detailed chemical reaction model developed in the present work (LLNL model). At temperatures above about 1250 K, the calculated data match the experimental ones while in a temperature range between 1000 K and 1250 K the measured data are overpredicted by about a factor of 2. At lower temperatures (< 1000 K), the deviations are smaller and in between the uncertainty range determined for the variation of the predicted ignition delay time for $p = p(t/s > 0) \pm 20\%$. Additionally, the effects of the reported fuel recovery rate of $(95 \pm 5)\%$ are

calculated with the LLNL model for a recovery rate of 90%, assuming total loss without conversion as indicated by the GC/MS-analysis, to introduce a deviation of the ignition delay times of +8% at 850 K and -7% at 1600 K (each at $\phi = 1$ and $\phi = 2$) crossing over at around 1230 K. Last but not least, the blast wave velocity is assigned an error of 30% affecting blast wave correction of side-on measured ignition delay times. As applied to the laminar flame speed measurements the error function approach from Olm et al. [52] yields an error function value of 19.3 at $\phi = 1$ and 36.1 at $\phi = 2$, whereas the average absolute deviation reads 3.3 at $\phi = 1$ and 4.6 at $\phi = 2$, respectively.

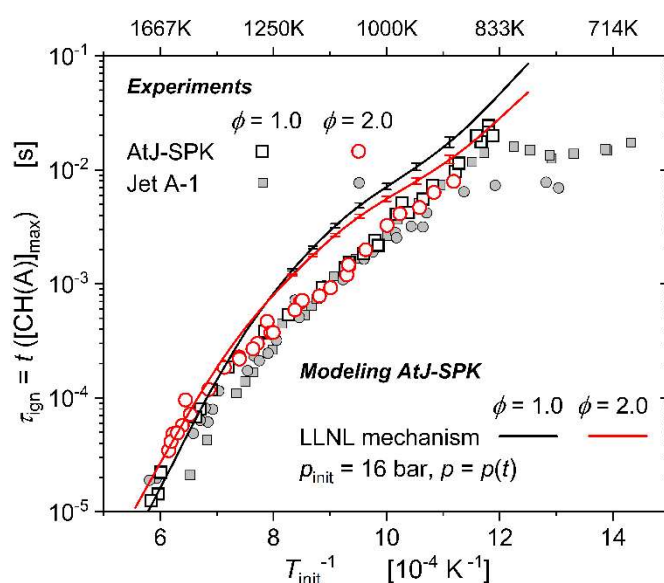


Figure 8 Comparison between measured (symbols) and calculated (curves) ignition delay times (τ_{ign}) of AtJ-SPK in air at stoichiometric and rich fuel-air ratios with a dilution of N_2 of 1:2. Calculations were performed using the LLNL reaction model developed within the present work. For comparison, measurements of Jet A-1 [11,12] are shown. Error bars shown as example at each ϕ value indicate a variation of the predicted ignition delay time for $p = p(t/s > 0) \pm 20\%$ at different initial temperatures.

For the purpose of a further validation of the LLNL model, the experimental shock tube data of Zhu et al. [6] and Flora et al. [7] as well as the RCM data of Valco et al. [9] were predicted as well. The results are presented in Fig. S7 of the Supplementary Material. The data of Flora et al. [7] measured at 16 atm as well as the RCM data of Valco et al. [9] measured at 20 bar are well reproduced

whereas the data of Zhu et al. [6] are predominantly overpredicted. Since Zhu et al. [6] conducted the measurements at pressures of 3 atm and 6 atm, this may be an indication that there is the need for further optimized mechanism for lower pressures. Overall, the modeling results show that the mechanism accurately covers a broad temperature range from about 600 K to more than 1700 K.

Comparison of the measured AtJ-SPK ignition delay time data to those of Jet A-1 experimentally determined previously [11,12] at the same conditions as applied within this work (Fig. 8) shows a quite similar result with a trend to slightly longer ignition delay times for AtJ-SPK. This corresponds to the findings from the measurements of the laminar burning velocities discussed above: Obviously, AtJ-SPK has a slightly lower reactivity than Jet A-1. For the ignition delay times, the most obvious difference occurs at $T < 850$ K where Jet A-1 shows a negative temperature coefficient (NTC)-behavior caused by the high n-alkane content of the crude oil-based fuel, thus giving rise to low-T alkylperoxy (“cool flame”) kinetics. In contrast, AtJ-SPK does not reveal an NTC-behavior at the chosen experimental conditions because it contains only highly branched molecules (alkanes only). Besides the fuel composition itself, this is the main difference between AtJ-SPK and Jet A-1 which affects clearly the ignition pattern of these two aviation fuels. A more detailed discussion on the influence of the molecule structure occurring in Gevo’s AtJ-SPK is given in section 4.4.

4.3 Kinetic analysis

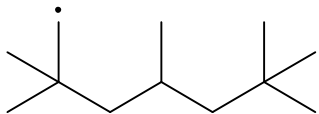
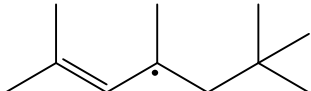
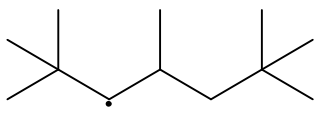
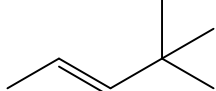
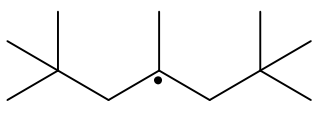
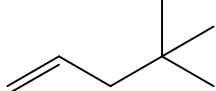
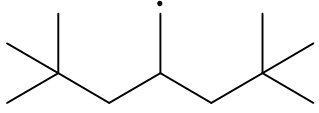
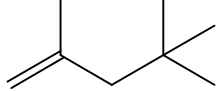
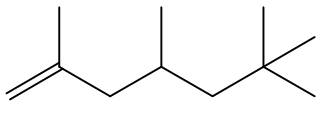
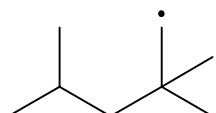
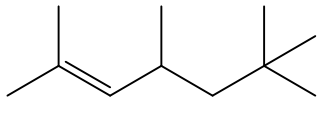
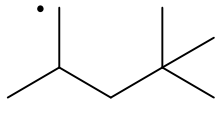
To identify the dominant chemistry as predicted by the detailed model developed within the present work, kinetic analyses have been conducted which include reaction flux analyses and brute force sensitivity analyses. These three different analyses are aimed to provide a detailed understanding of the important chemistry as predicted by the detailed mechanism.

4.3.1 Reaction flux analyses

To understand the oxidation pathways of the Gevo-fuel, we conducted a reaction path analysis starting with an initial temperature, pressure, and fuel/oxidizer equivalence of 1100 K, 16 bar and $\phi = 2$

respectively. An initial temperature of 1100 K was chosen as it is close to mean of the inverse temperature investigated on the Arrhenius plot shown in Fig. 8. The flux analysis was conducted at a time instant corresponding to that of fuel conversion of 50%. This time was selected to understand the chemistry during the induction time and far away from thermal run-away. Summary of the flux analysis results are shown in Fig. 9. We show the flux analysis of iso-dodecane which constituents about 83% of the fuel surrogate and for sake of clarity we list the structure and the chemical name of the larger intermediates (> 5 carbons) found important from flux analysis in Tab. 4.

Table 4 Structure and chemical name of the species (as used in mechanism) found to be important during oxidation of iso-dodecane at high temperatures.

Structure	Species name	Structure	Species name
	X1C12H25		XC11H21
	X2C12H25		NEC7D3
	X3C12H25		NEC7D4
	X4C12H25		IC8D4
	X1C11H22		IC8-1R
	X2C11H22		IC8-5R

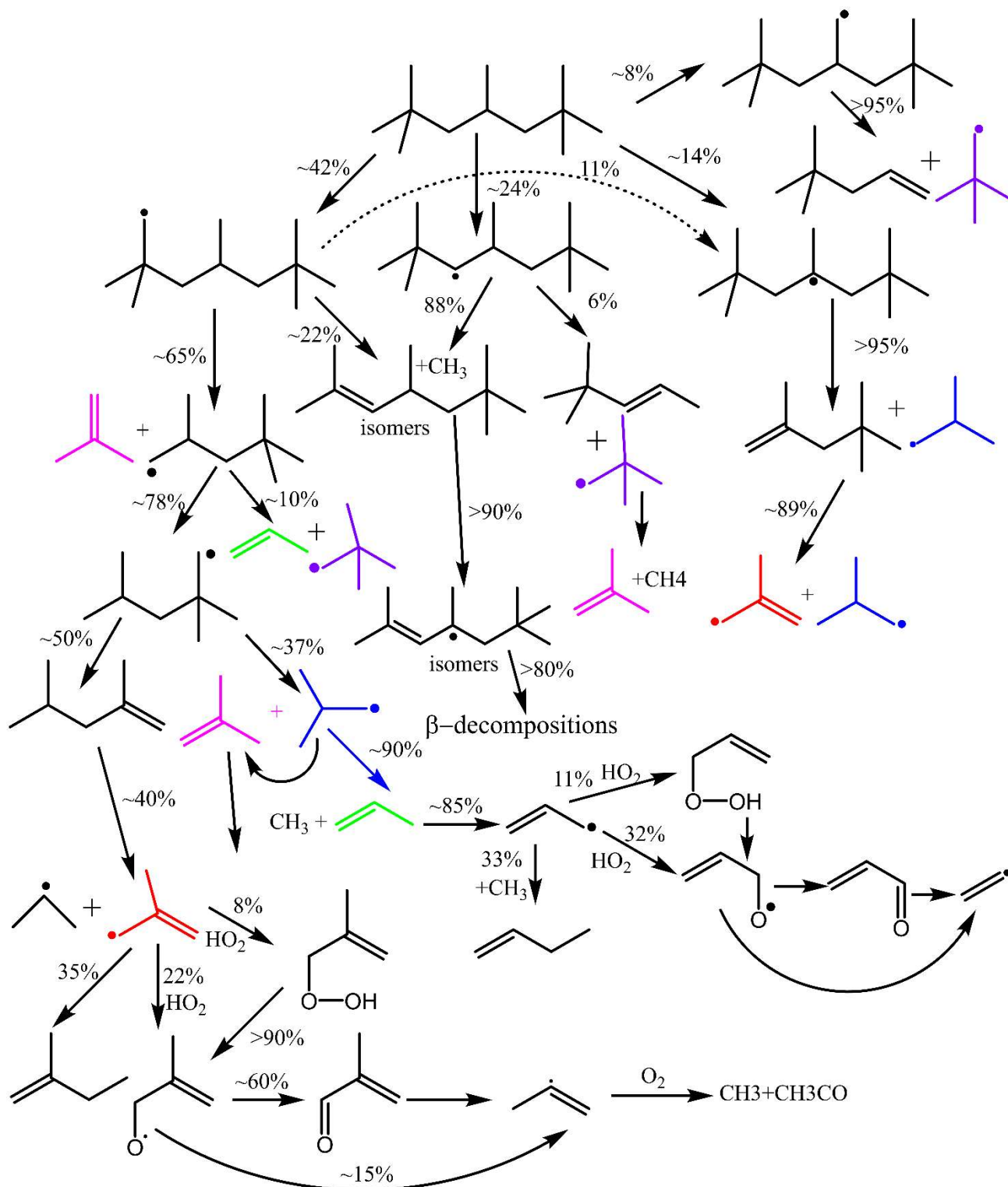


Figure 9 Plot showing the important reaction pathways in oxidation of Gevo-AtJ surrogate fuel. Flux analysis conducted at 50% conversion of iso-dodecane with initial pressure, temperature, and equivalence ratio of 16 bar, 1100 K, and $\phi = 2$.

The flux analysis shows that the fuel consumption is dominated by the H-abstraction reactions by OH, HO₂, CH₃, H, and O radicals, of which the abstraction by OH and HO₂ are found to be dominant. The H-abstraction reactions lead to formation of the four different radicals of iso-dodecane, the abstractions from the methyl substitutions on the ter-butyl functionality producing the primary radicals (X1C12H25) dominate with a consumption flux of about 42% followed by abstractions from secondary sites producing secondary iso-dodecane radical (X2C12H25) which represents about 24% of the flux. The abstractions from the tertiary and the symmetric methyl site producing X3C12H25, X4C12H25 radicals were found to contribute to about 14% and 8% of the consumption.

All the four iso-dodecane radicals are predominantly consumed by unimolecular β -scission reactions producing smaller hydrocarbon fragments. About 60% of X1C12H25 radical produced undergoes β -scissions to iso-butene+5-isooctyl radical (IC8-5R), the 5-isooctyl radical subsequently undergoes a unimolecular isomerization reaction to produce 1-isooctyl radical (IC8-1R). IC8-1R undergoes β -scissions producing neo-heptene (NEC7D3). +CH₃ (~50% of flux), and iso-butene+iso-butyl radical (37%). The other important reactions of X1C12H25 radical include formation of iso-undecenes (X1C11H22) + CH₃ and isomerization to X3C12H25 radicals. Iso-undecene isomers are also produced from β -scissions reactions of X2C12H25 radicals. Of the different iso-undecene isomers, the selectivity towards formation of X2C11H22 isomer is higher. These iso-undecene isomers are consumed by H-abstraction reactions to produce both the allylic and non-allylic C11H21 radicals. In the present mechanism, the formation of different C11H21 radicals are not considered to reduce the complexity, and all the radicals are represented using on lumped radical XC11H21. The XC11H21 radicals produced undergo β -scissions to produce 2-methyl-1,3 pentadiene (IC6D13), 2,4-dimethyl-1,3 pentadiene (I24C7D13), iso-butyl radicals and neo-pentyl radicals. The tertiary iso-dodecyl radicals, X3C12H25, undergo decomposition reactions to produce iso-butyl radical along with di-isobutylene isomer. Di-isobutylene isomer at the current conditions undergoes unimolecular decomposition to produce iso-butyl radical along with 2-methyl-allyl radical (IC4H7). The symmetric primary iso-dodecyl radical undergoes unimolecular decomposition leading to formation of neo-pentyl

radical and neo-heptene (NEC7D4). The neo-pentyl radical undergoes β -scissions to produce isobutene along with methyl radical, while neo-heptene undergoes unimolecular decomposition to produce ter-butyl radical along with allyl radical.

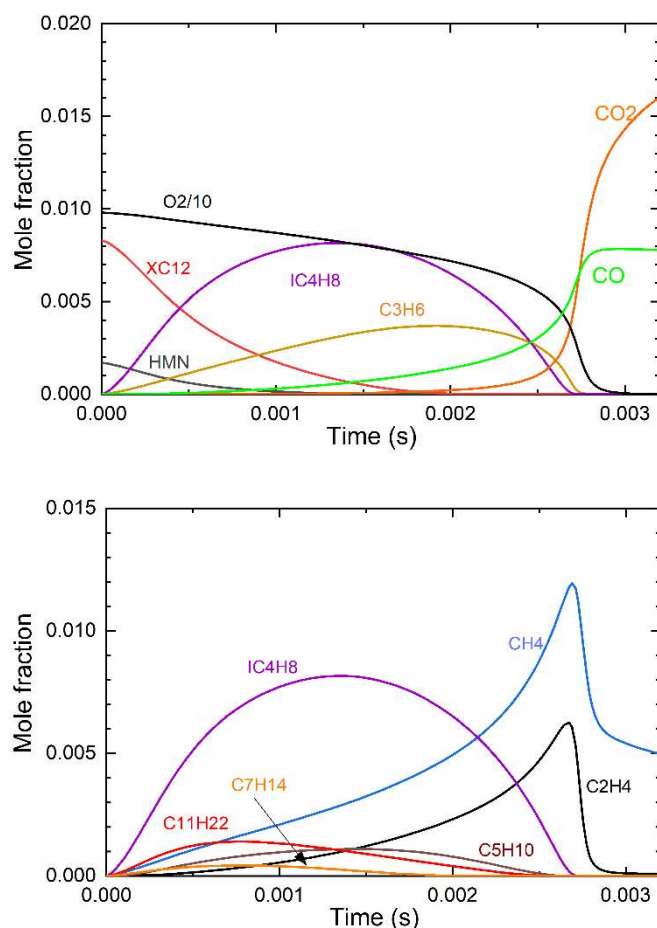


Figure 10 Plots showing the consumption of parent fuels (iso-dodecane: XC12, iso-cetane: HMN), the evolution of different intermediates and formation of carbon oxides.

From flux analysis it can be inferred that (i) the parent fuel chemistry is dominating the formation of fuel-radicals which predominantly undergo β -scissions reactions producing smaller C_1 - C_8 intermediates along with C_{11} intermediates and that (ii) the flux through reactions of fuel radicals with O_2 or HO_2 are very minimal at the present temperature of interest. The C_3 - C_{11} intermediates further undergo decomposition reactions producing smaller C_1 - C_2 fragments which react with O_2 and HO_2 and control the global oxidation of the fuel. To support this assertion that global oxidation is controlled

by oxidation of the smaller fragments we plot the mole fraction profiles of the fuel, O₂, and different intermediates in Fig. 10. As seen in this figure, the consumption of parent fuels, iso-dodecane (XC12) and iso-cetane (HMN), lead to build of propene, iso-butene, iso-pentenes, iso-heptenes, and iso-undecenes till 1.5 ms during which the consumption of oxygen is only about 13%. The buildup of CO which is an indicator of initiation of oxidation is controlled by the consumption of iso-butene and propene. Oxidation of radicals of iso-butene and propene lead to formation of methane, ethylene, and their radicals. The oxidation of methyl and vinyl radicals triggered by decomposition of H₂O₂ leads to global oxidation.

4.3.2 Brute force sensitivity analyses

Brute force sensitivity analyses were conducted at two initial temperatures, 900 K and 1300 K, for the stoichiometric mixture at high pressure ($p = 16$ bar). The results are displayed in Fig. 11 with showing the ten most sensitive reactions at each considered temperature. At 900 K, the most sensitive reaction is the decomposition of H₂O₂ to OH radicals which results in accelerating the ignition process. The further reactions highlight the large importance of HO₂ radicals at these conditions. The reactions of HO₂ with a fuel molecule, e.g. $\text{XC}_{12}\text{H}_{26} + \text{HO}_2 \Leftrightarrow \text{X2C}_{12}\text{H}_{25} + \text{H}_2\text{O}_2$, lead to an acceleration of the ignition, while the consumption of HO₂ leading to formation of stable products ($\text{CH}_3 + \text{HO}_2 \Leftrightarrow \text{CH}_4 + \text{O}_2$ and $\text{HO}_2 + \text{HO}_2 \Leftrightarrow \text{H}_2\text{O}_2 + \text{O}_2$) decelerates ignition. Also, it is worth noting that at $T = 900$ K, reactions of fuel molecules show up as sensitive reactions. This suggests that the oxidation of smaller fragments produced from breakdown of fuel molecules is not the only rate limiting step within the global oxidation of the fuel at these low-to-intermediate temperatures.

Similar to the sensitivity analysis of the laminar flame speed, the most sensitive reaction at higher temperatures (1300 K) is $\text{O}_2 + \text{H} \Leftrightarrow \text{O} + \text{OH}$ which accelerates the ignition process being a chain-branching reaction. Due to the higher temperature, reactions of fuel molecules and fuel radicals, respectively, are found to be not sensitive. Similar to the results of the sensitivity analysis done at 900 K, reactions containing HO₂ are predominant due to the high pressure (16 bar). Here, the reaction

$\text{CH}_3 + \text{HO}_2 \rightleftharpoons \text{CH}_4 + \text{O}_2$ is the most important one among the decelerating reactions. In contrast to this, the reaction $\text{CH}_3 + \text{HO}_2 \rightleftharpoons \text{CH}_3\text{O} + \text{OH}$ contributes to the acceleration of the ignition, being a chain-branching reaction.

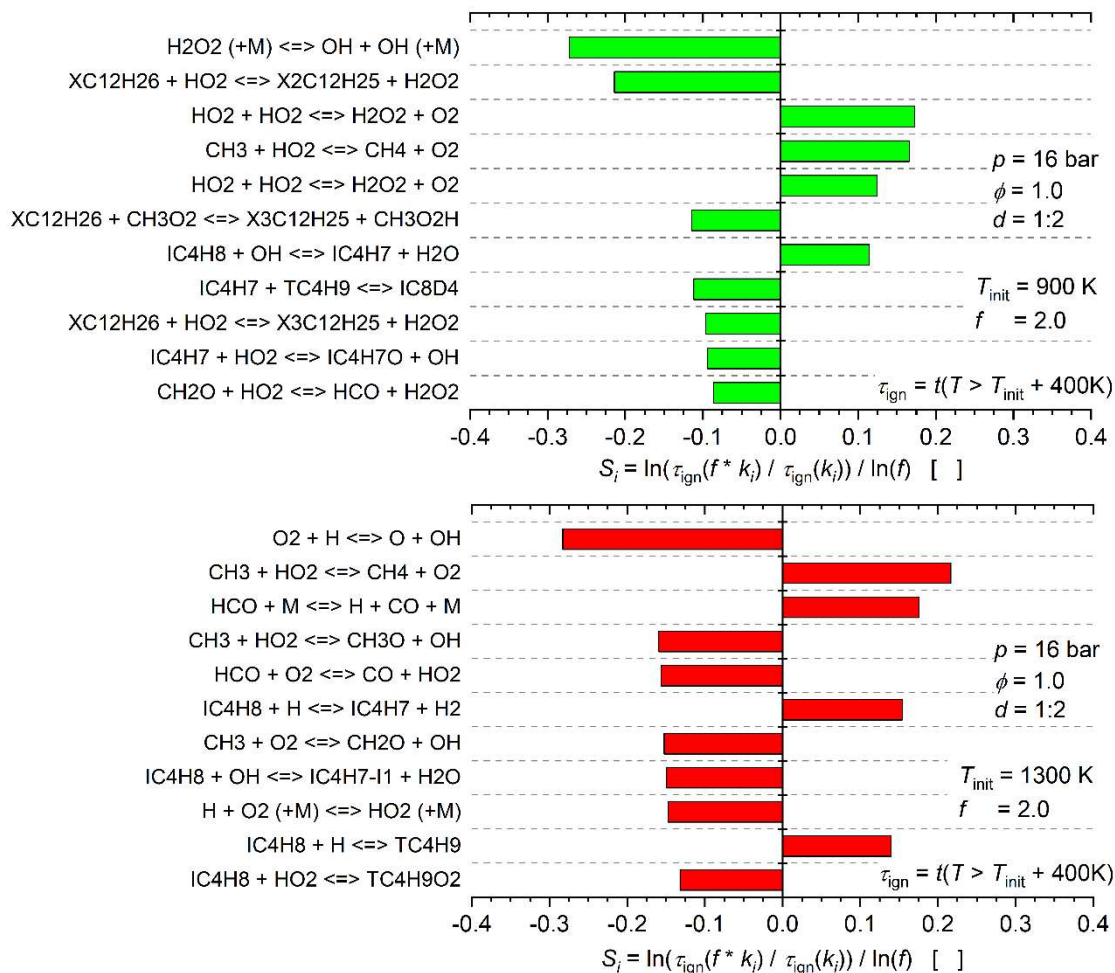


Figure 11 Brute force sensitivity analyses of ignition delay times (τ_{ign}) for stoichiometric high-pressure ($p = 16 \text{ bar}$) fuel-air mixtures at $T = 900 \text{ K}$ (top) and $T = 1300 \text{ K}$ (bottom); S_i – sensitivity coefficient for reaction “ i ”, d – dilution, f – factor for perturbation of the reaction rates in mechanism.

4.4 Influence of branched fuel molecules on the ignition delay time

The present AtJ-SPK fuel consists of two rather large, highly branched alkane fuels, as illustrated in Fig. 1. Further Gevo fuel components from other studies [4] include iso-octane (2,2,4-trimethyl pentane, $i\text{-C}_8\text{H}_{18}$), iso-tridecane (2,6,8-trimethyl decane, $i\text{-C}_{13}\text{H}_{28}$), and iso-nonane (2,2,3,3-

tetramethyl pentane, $i\text{-C}_9\text{H}_{20}$), all of which are also large, highly branched alkane molecules with three or four side methyl radical branches. Each methyl radical has three H atoms held tightly at primary C-H bonds, discouraging intramolecular abstraction necessary to support low temperature, “cool flame” reactions. In addition, none of these fuels contains a linear carbon atom chain; long, linear carbon atom chains of $-\text{CH}_2-$ groups, such as those in n-alkane molecules, that strongly support robust low temperature intramolecular reaction pathways that encourage high reactivity and cool flames. Primary Reference Fuels (PRF) for gasoline and diesel fuel employ iso-octane and iso-cetane as the relatively low-reactivity components of these reference fuels, and their low reactivity under engine combustion conditions is due to the presence of numerous methyl side chains and the absence of extended linear carbon atom chains.

The detailed kinetic reaction mechanisms for iso-dodecane (2,2,4,6,6-pentamethyl heptane, $i\text{-C}_{12}\text{H}_{26}$), and iso-cetane (2,2,4,4,6,8,8-heptamethyl nonane, $i\text{-C}_{16}\text{H}_{34}$), the major components of the AtJ-SPK Gevo isoparaffinic fuel, were used to examine the details of the reaction pathways that control their ignition delay times. Their ignitions were computed for a model problem that has been used widely to study the influence of molecular structure on ignition. The original experiments were carried out within pioneering work by Adomeit et al. [53,54] who studied the ignition of stoichiometric mixtures of n-heptane, iso-octane, and n-decane with air at 13.5 and 40 bar pressures, under reflected shock wave conditions with initial post shock wave temperatures from 660 to 1350 K. That work demonstrated the existence of a pronounced Negative Temperature Coefficient (NTC) from 800 - 1000 K in the ignition delay time for n-heptane, while iso-octane produced only a very slight NTC behavior at lower temperatures from 650-750 K. These reaction conditions have been very instructive for many past studies to study the influence of molecular structure on ignition of isomers of heptane [55], alkyl esters in biodiesel fuels [56,57], and many n-alkane and 2-methyl alkane fuels [22].

Ignition delay times were computed for these test conditions with the same kinetic reaction mechanism used in the present study of the AtJ-SPK fuels, and the results for iso-cetane and iso-

dodecane are shown in Fig. 12, together with results under the same conditions for iso-octane and n-heptane, the PRFs for gasoline. For comparison, also the experimental data of AtJ-SPK from the present work and of iso-octane [11] are shown in Fig. 12. Iso-octane were measured at 16 bar as well and at the same shock tube as the AtJ-SPK fuel; the data are given in the supplementary material (SM2, Tab. S11). The difference between the pressure used for the modeling (13.6 bar) and the measurements (16 bar) amounts to 15% being less than the maximum uncertainty range from the experiment $\pm 20\%$ (see section 4.2).

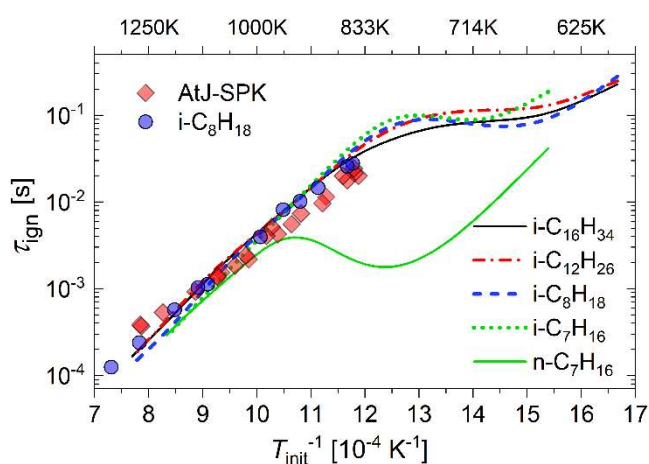
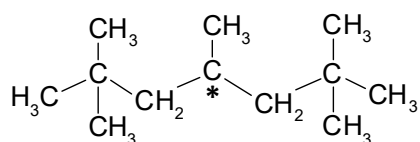


Figure 12 Computed ignition delay times (lines) for stoichiometric fuel-air mixtures at $p = 13.6$ bar and $\phi = 1.0$ for iso-cetane (2,2,4,4,6,8,8-heptamethyl nonane, $i\text{-C}_{16}\text{H}_{34}$), iso-dodecane (2,2,4,6,6-pentamethyl heptane, $i\text{-C}_{12}\text{H}_{26}$), iso-octane (2,2,4-trimethyl pentane, $i\text{-C}_8\text{H}_{18}$), iso-heptane (2,2,3-trimethyl butane, $i\text{-C}_7\text{H}_{16}$), and n-heptane ($n\text{-C}_7\text{H}_{16}$), using the LLNL detailed kinetic mechanism. The shown experimental data (dots) of AtJ-SPK (present work) and iso-octane [11] were measured at $p = 16$ bar, corresponding to a deviation of $\pm 15\%$ compared to $p = 13.6$ bar.

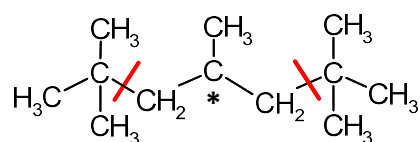
Only n-heptane shows a significant NTC behavior for these conditions, between 800 and 950 K; the close scrutiny of the ignition delay times for the other fuels shows minor NTC behavior for the iso-octane fuel at temperatures much lower than the NTC region for n-heptane, and little or no NTC behavior for iso-cetane ($i\text{-C}_{16}\text{H}_{34}$) and iso-dodecane ($i\text{-C}_{12}\text{H}_{26}$). For further comparison, ignition delay

times were also computed for the most heavily branched isomer of heptane, specifically 2,2,3-trimethyl butane, and those results are also included in Fig. 12, showing a similarly very small amount of NTC behavior between 700 and 800K.

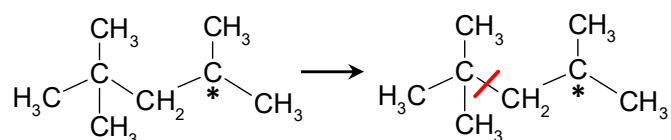
All four heavily branched alkane fuels show long ignition delay times in Fig. 12, which are very similar for all temperatures, especially for temperatures above about 700 K, with little or no NTC behavior at these pressures, while the only long-chain fuel n-heptane have ignition delay times that are qualitatively and quantitatively much different from those of the highly branched fuels. The dominant intermediate species produced by all of the highly branched fuels is iso-butene (i-C₄H₈), which can easily be seen from a simple inspection of these fuel structures. For example, with i-C₁₂H₂₆ (2,2,4,6,6-pentamethyl heptane) where the * indicates a radical site:



the most energetically favored H atom abstraction reaction is the only H atom located at a tertiary site, the '4' site, and when that is followed by β -scission of the resulting radicals, the result



(X4C12H25 = IC8D4 + ter-butyl radical) produces a tert-butyl radical that subsequently decomposes to an iso-butene, and di-isobutylene (IC8D4). IC8D4 decomposes to 2-methyl allyl radical (iso-butenyl radical) and ter-butyl radical. The same type of radical decomposition, this time for iso-octane follows abstraction of the only H atom bound at a weak tertiary site is:



(IC8-4R = iso-butene + ter-butyl radical) followed by β -scission of the resulting radical, results in iso-butene and a tert-butyl radical which then decomposes to produce another iso-butene species.

Similar structural analysis of the iso-cetane fuel molecule shows the same overall high fraction of iso-butene intermediates and the low reactivity shown for iso-cetane (Fig. 12). The only large fuel with dramatically shorter ignition delay times given in Fig. 12, for n-heptane, produces very low amounts of either iso-butene or methyl radicals as intermediate species, while ethene (C_2H_4) is its dominant intermediate species, and ethene is highly reactive. The high levels of ethene and the absence of iso-butene as reaction intermediates are common to the ignition of n-alkane fuels and all other fuels with linear chains of carbon atoms such as 2-methyl alkanes [22]. Long linear chains of $-CH_2-$ groups of carbon atoms, with their relatively weak secondary C-H bonds, are generally responsible for high levels of low temperature chain branching and high rates of cool flame reactions, while highly branched, large fuel molecules such as those found in Gevo AtJ fuels avoid significant low temperature ignition with ignition properties very similar to those of iso-octane.

The features summarized above explain why so many of the large, highly branched alkane fuels have such similar ignition delay times and why the HyChem approach [10,49] is successful for prediction of ignition under compression for these fuels. Each of these highly branched alkane fuels has a preferential weak tertiary or secondary C-H site for initial H atom abstraction, with most or all subsequent β -scission reactions leading to iso-butene, or alternatively to neo-pentyl radicals which rapidly decompose to iso-butene. Thus, the collection of products of the initial reaction pathways of all of these highly branched alkane fuels are remarkably similar, and their subsequent reaction pathways are therefore very similar and have very similar computed ignition delay times, as illustrated in Fig. 12, and it can be noted that, on the basis of current modeling capabilities, all of the present family of Gevo AtJ fuels appear to be essentially kinetically interchangeable.

5. CONCLUSIONS

In this work, an experimental and modeling study of a highly-branched iso-paraffinic AtJ-SPK, a sustainable aviation fuel, is presented. The performed experiments include laminar burning velocities measured at pressures of 1 and 3 bar at a preheat temperature of 473 K as well as ignition delay times of stoichiometric ($\phi = 1.0$) and fuel-rich mixtures ($\phi = 2.0$) measured behind reflected shock waves at an initial pressure of 16 bar and temperatures ranging from about 850 K up to about 1700 K at a dilution with nitrogen (1:2). For comparison, Jet A-1 was measured at the same conditions as AtJ-SPK. The results show that the combustion behavior of AtJ-SPK is very similar to Jet A-1 revealing a slight trend towards a lower reactivity, for temperatures higher than about 850 K.

Within the modeling study, a new reaction mechanism for AtJ-SPK (LLNL model) was developed based on the reaction class approach introduced by Curran et al. [30,31]. This new mechanism being able to predict the experimental data consists of 1832 species and 7337 reactions. Especially the experimental ignition delay time data obtained at higher pressures of about 16 bar and the laminar flame speed data, at ambient pressure, are satisfactorily reproduced by the mechanism. The detailed chemical kinetic mechanism is able to better predict burning velocities, with room for improvements at higher pressures and higher values of fuel-air equivalence ratio. This reaction mechanism represents a significant advance in modeling ignition of branched chain hydrocarbon that has been further validated in this work as well as a major advance towards an ability to simulate combustion of much larger and more complex hydrocarbon fuels with multiple side chains. Within the mechanism development and validation, iso-butene is identified as a key intermediate species playing the significant role in highly branched fuels. Further works will focus on the mechanism optimization to resolve the discrepancies as well as on the mechanism reduction with the aim to reduce computational time and make the mechanism applicable for the use in CFD simulations.

ACKNOWLEDGEMENTS

The authors (DLR) thank N. Ackermann and H. Dreyer for their help towards the experiments on ignition delay times and the Bundeswehr Research Institute for Materials, Fuels, and Lubricants (WIWeB) for providing us with Alcohol-to-Jet SPK and Jet A-1. Part of the computational part of this work was carried out under the auspices of the US Department of Energy by Lawrence Livermore National Laboratory under Contract DE-AC52-07NA27344 and was supported by the US Department of Energy, Office of Vehicle Technologies.

REFERENCES

- [1] ATAG (Aviation Transport Action Group), Aviation: Benefits Beyond Borders, Full Report (2020), available at <https://aviationbenefits.org/downloads/aviation-benefits-beyond-borders-2020/> (access 26th January 2021).
- [2] M. Kousoulidou, L. Lonza, Biofuels in aviation: Fuel demand and CO₂ emissions evolution in Europe toward 2030, *Transp. Res. Part D* 46 (2016) 166-181.
- [3] ASTM D7566, Standard Specification for Aviation Turbine Fuel Containing Synthesized Hydrocarbons, available at <https://www.astm.org/Standards/D7566.htm> (access 26th January 2021).
- [4] J. Guzman, G. Kukkadapu, K. Brezinsky, C.K. Westbrook, Experimental and modeling study of the pyrolysis and oxidation of an iso-paraffinic alcohol-to-jet fuel, *Combust. Flame* 201 (2019) 57-64.
- [5] S.H. Won, P.S. Veloo, S. Dooley, J. Santner, F.M. Haas, Y. Ju, F.L. Dryer, Predicting the global combustion behaviors of petroleum-derived and alternative jet fuels by simple fuel property measurements, *Fuel* 168 (2016) 34-46.
- [6] Y. Zhu, S. Li, D.F. Davidson, R.K. Hanson, Ignition delay times of conventional and alternative fuels behind reflected shock waves, *Proc. Combust. Inst.* 35 (2015) 241-248.

- [7] G. Flora, J. Balagurunathan, S. Saxena, J.P. Cain, M.S.P. Kahandawala, M.J. DeWitt, S.S. Sidhu, E. Corporan, Chemical ignition delay of candidate drop-in replacement jet fuels under fuel-lean conditions: A shock tube study, *Fuel* 209 (2017) 457-472.
- [8] K. Min, D. Valco, A. Oldani, T. Lee, An ignition delay study of category A and C aviation fuel, *Proc. ASME 2015 IMECE2015*, Vol. 6A: Energy, Paper No.: IMECE2015-51713.
- [9] D. Valco, K. Min, A. Oldani, T. Edwards, T. Lee, Low temperature autoignition of conventional jet fuels and surrogate jet fuels with targeted properties in a rapid compression machine, *Proc. Combust. Inst.* 36 (2017) 3687-3694.
- [10] K. Wang, R. Xu, T. Parise, J. Shao, A. Movaghar, D.J. Lee, J.-W. Park, Y. Gao, T. Lu, F.N. Egolfopoulos, D.F. Davidson, R.K. Hanson, C.T. Bowman, H. Wang, A physics-based approach to modeling real-fuel combustion chemistry – IV. HyChem modeling of combustion kinetics of a bio-derived jet fuel and its blends with a conventional Jet A, *Combust. Flame* 198 (2018), 477-489.
- [11] M. Braun-Unkhoff, T. Kathrotia, S. Richter, C. Naumann, N. Slavinskaya, T. Methling, U. Riedel, Reaction Model Development for Synthetic Jet Fuels – Surrogate Fuels as a Flexible Tool to Predict their Performance, *Proc. ASME Turbo Expo 2018*, GT2018-76997, doi: 10.1115/GT2018-76997.
- [12] C. Naumann, T. Kathrotia, F. Herrmann, S. Richter, M. Braun-Unkhoff, U. Riedel, Synthetische Treibstoffe – Einfluß des Aromatengehaltes auf die Rußbildung („SynTreAmR“), final project report for Wehrwissenschaftliches Institut für Werk- und Betriebsstoffe (WIWeB), Erding, Germany (2018).
- [13] S. Richter, T. Kathrotia, C. Naumann, T. Kick, N. Slavinskaya, M. Braun-Unkhoff, U. Riedel, Experimental and modeling study of farnesane, *Fuel* 215 (2018) 22-29.
- [14] T. Kick, J. Herbst, T. Kathrotia, J. Marquetand, M. Braun-Unkhoff, C. Naumann, U. Riedel, An experimental and modeling study of burning velocities of possible future synthetic jet fuels, *Energy* 43 (1) (2012) 111-123.

- [15] G. Andrews, D. Bradley, Determination of burning velocities: A critical review, *Combust. Flame* 18 (1) (1972) 133-153.
- [16] H. Eberius, T. Kick, Stabilization of premixed, conical methane flames at high pressure, *Ber. Bunsenges. Phys. Chem.* 96 (10) (1992) 1416-1419.
- [17] P. Dagaut, F. Karsenty, G. Dayma, P. Diévert, K. Hadj-Ali, A. Mzé-Ahmed, M. Braun-Unkhoff, J. Herzler, T. Kathrotia, T. Kick, C. Naumann, U. Riedel, L. Thomas, Experimental and detailed kinetic model for the oxidation of a Gas to Liquid (GtL) jet fuel, *Combust. Flame* 161 (3) (2014) 835-847.
- [18] T. Kathrotia, C. Naumann, P. Oßwald, M. Köhler, U. Riedel, Kinetics of Ethylene Glycol: The first validated reaction scheme and first measurements of ignition delay times and speciation data, *Combust. Flame* 179 (2017) 172-184.
- [19] J. Herzler, L. Jerig, P. Roth, Shock tube study of the ignition of lean n-heptane/air mixtures at intermediate temperatures and high pressures, *Proc. Combust. Inst.* 30 (2005) 1147-1153.
- [20] P. Roth, Vergleichende Messungen der Schwingungsenergie-Anregung von CO hinter Stoßwellen und der Schwingungsenergie-Abregung in Expansionswellen, Forschungsbericht 71-62, Deutsche Forschungs- und Versuchsanstalt für Luft- und Raumfahrt e.V., Institut für Reaktionskinetik, Stuttgart, Germany, 1971.
- [21] C.K. Westbrook, W.J. Pitz, O. Herbinet, H.J. Curran, E.J. Silke, A Comprehensive Detailed Chemical Kinetic Reaction Mechanism for Combustion of n-Alkane Hydrocarbons From n-Octane to n-Hexadecane, *Combust. Flame* 156 (2009) 181-199.
- [22] S.M. Sarathy, C.K. Westbrook, M. Mehl, W.J. Pitz, C. Togbe, P. Dagaut, H. Wang, M.A. Oehlschlaeger, U. Niemann, K. Seshadri, P.S. Veloo, F.N. Egolfopoulos, T. Lu, Comprehensive chemical kinetic modeling of the oxidation of 2-methyl alkanes from C₇ to C₂₀, *Combust. Flame* 158 (2011) 2338-2357.
- [23] R. Fang, G. Kukkadapu, M. Wang, S.W. Wagnon, K. Zhang, M. Mehl, C.K. Westbrook, W.J. Pitz, C.J. Sung, Fuel molecular structure effect on autoignition of highly branched iso-alkanes at low-

- to-intermediate temperatures: iso-octane versus iso-dodecane, *Combust. Flame* 214 (2020) 152-166.
- [24] M.A. Oehlschlaeger, J. Steinberg, C.K. Westbrook, W.J. Pitz, The Autoignition of iso-Cetane at High to Moderate Temperatures and Elevated Pressures: Shock Tube Experiments and Kinetic Modeling, *Combust. Flame* 156 (2009) 2165-2172.
- [25] G. Kukkadapu, C.J. Sung, Autoignition study of binary blends of n-dodecane/1-methylnaphthalene and iso-cetane/1-methylnaphthalene, *Combust. Flame* 189 (2018) 367-377.
- [26] J. Bugler, K.P. Somers, E.J. Silke, H.J. Curran, Revisiting the kinetics and thermodynamics of the low-temperature oxidation pathways of alkanes: A case study of the three pentane isomers, *J. Phys. Chem. A* 119 (28) (2015) 7510-7527.
- [27] K. Zhang, C. Banyon, U. Burke, G. Kukkadapu, S.W. Wagnon, M. Mehl, H.J. Curran, C.K. Westbrook, W.J. Pitz, An experimental and kinetic modeling study of the oxidation of hexane isomers: Developing consistent reaction rate rules for alkanes, *Combust. Flame* 206 (2019) 123-137.
- [28] N.M. Atef, G. Kukkadapu, S.Y. Mohamed, M. Al Rachidi, C. Banyon, M. Mehl, A. Heufer, E.F. Nasir, A. Alfazazi, A.K. Das, C.K. Westbrook, W.J. Pitz, T. Lu, A. Farooq, C.-J. Sung, H.J. Curran, S.M. Sarathy, A comprehensive iso-octane combustion model with improved thermochemistry and chemical kinetics, *Combust. Flame* 178 (2017) 111-134.
- [29] Y. Li, C.-W. Zhou, K.P. Somers, K. Zhang, H.J. Curran, The oxidation of 2-butene: A high pressure ignition delay, kinetic modeling study and reactivity comparison with isobutene and 1-butene, *Proc. Combust. Inst.* 36 (1) (2017) 403-411.
- [30] S.M. Burke, J.M. Simmie, H.J. Curran, Critical evaluation of thermochemical properties of C1-C4 species: Updated group-contributions to estimate thermochemical properties, *J. Phys. Chem. Ref. Data* 44 (1) (2015) 013101.
- [31] H.J. Curran, P. Gaffuri, W.J. Pitz, C.K. Westbrook, A Comprehensive Modeling Study of n-Heptane Oxidation, *Combust. Flame* 114 (1998) 149-177.

- [32] H.J. Curran, P. Gaffuri, W.J. Pitz, C.K. Westbrook, A Comprehensive Modeling Study of iso-Octane Oxidation, *Combust. Flame* 129 (2002) 253-280.
- [33] M. Mehl, W.J. Pitz, C.K. Westbrook, H.J. Curran, Kinetic modeling of gasoline surrogate components and mixtures under engine conditions, *Proc. Combust. Inst.* 33 (2011) 193-200.
- [34] J. Badra, A. Farooq, Site-specific reaction rate constant measurement for various secondary and tertiary H-abstraction by OH radicals, *Combust. Flame* 162 (2015) 2034-2044.
- [35] S. Sharma, S. Raman, W.H. Green, Intramolecular Hydrogen Migration in alkylperoxy and hydroperoxyalkylperoxy radicals: Accurate treatment of hindered rotors, *J. Phys. Chem. A* 114 (2010) 5689-5701.
- [36] S.M. Villano, L.K. Huynh, H.H. Carstensen, and A.M. Dean, High-pressure rate rules for alkyl + O₂ reactions. 1. The dissociation, concerted elimination, and isomerization channels of the alkyl peroxy radical, *J. Phys. Chem. A* 115 (2011) 13425-13442.
- [37] S. Villano, L.K. Huynh, H.-H. Carstensen, A.M. Dean, High-pressure rate rules for alkyl+O₂ reactions. 2. The isomerization, cyclic ether formation, and β -scission reactions of hydroperoxy alkyl radicals, *J. Phys. Chem. A* 116 (2012) 5068-5089.
- [38] A. Miyoshi, Systematic computational study on the unimolecular reactions of Alkylperoxy (RO₂), hydroperoxyalkyl (QOOH), and hydroperoxyalkylperoxy (O₂QOOH) radicals, *J. Phys. Chem. A* 115 (2011) 3301-3325.
- [39] A.W. Jasper, S.J. Klippenstein, L.B. Harding, Theoretical rate coefficients for the reaction of methyl radical with hydroperoxyl radical and for methylhydroperoxide decomposition, *Proc. Combust. Inst.* 32 (2009) 279-286.
- [40] C.F. Goldsmith, M.P. Burke, Y. Georgievskii, S.J. Klippenstein, Effect of non-thermal product energy distributions on ketohydroperoxide decomposition kinetics, *Proc. Combust. Inst.* 35 (2015) 283-290.
- [41] N.J. Killingsworth, M.J. McNenly, R.A. Whitesides, S.W. Wagon, Cloud based tool for analysis of chemical kinetic mechanisms, *Combust. Flame* 221 (2020) 170-179.

- [42] S. Lapointe, R.A. Whitesides, M.J. McNenly, Sparse, iterative simulation methods for one-dimensional laminar flames, *Combust. Flame* 204 (2019) 23-32.
- [43] M.J. McNenly, R.A. Whitesides, D.L. Flowers, Faster solvers for large kinetic mechanisms using adaptive preconditioners, *Proc. Combust. Inst.* 35 (2015) 581-587.
- [44] Chemkin-Pro 15092, Reaction Design: San Diego, 2009.
- [45] A. E. Lutz, R. J. Kee, J. A. Miller, SENKIN: A FORTRAN program for predicting homogeneous gas phase chemical kinetics with sensitivity analysis, Sandia National Laboratories, Livermore, CA 94551-0969, report SAND 1988 87-8248.
- [46] R. Kee, F. Rupley, J. A. Miller, SAND89-8009, Sandia National Laboratories: Livermore, CA (USA) (1989).
- [47] J. Herzler, C. Naumann, Shock Tube Study of the Influence of NO_x on the Ignition Delay Times of Natural Gas at High Pressure. *Combust. Sci. Technol.* 184 (2012) 1635-1650.
- [48] T. Kathrotia, S. Richter, C. Naumann, N. Slavinskaya, T. Methling, M. Braun-Unkhoff, U. Riedel, Reaction Model Development for Synthetic Jet Fuels: Surrogate Fuels As a Flexible Tool to Predict Their Performance, *Proc. ASME Turbo Expo 2018 (Vol. 3) Oslo, Norway. June 11-15, 2018.* <https://doi.org/10.1115/GT2018-76997>.
- [49] S.H. Won, F.M. Haas, A. Tekawade, G. Kosiba, M.A. Oehlschlaeger, S. Dooley, F.L. Dryer, Combustion characteristics of C₄ iso-alkane oligomers: Experimental characterization of iso-dodecane as a jet fuel surrogate component, *Comb. Flame* 165 (2016) 137-143.
- [50] M. Braun-Unkhoff, T. Kathrotia, B. Rauch, U. Riedel, About the interaction between compositions and performance of alternative jet fuels, *CEAS Aeronautical J.* 7 (2016) 83-94.
- [51] C.K. Law C.K., *Combustion Physics*, Cambridge University Press, Cambridge, U.K., 2006.
- [52] C. Olm, I. Zsély, R. Pálvolgy, T. Varga, T. Nagy, H. Curran, T. Turányi, Comparison of the performance of several recent hydrogen combustion mechanisms, *Comb. Flame* 161 (9) (2014) 2219-2234.

- [53] H. Ciezki, G. Adomeit, Shock tube ignition of self-ignition of n-heptane-air mixtures under engine relevant conditions, *Combust. Flame* 93 (1993) 421-433.
- [54] K. Fieweger, R. Blumenthal, G. Adomeit, Self-ignition of S.I. Engine Model Fuels: A shock tube investigation at high pressure, *Combust. Flame* 109 (1997) 599-619.
- [55] C.K. Westbrook, W.J. Pitz, M. Mehl, H.J. Curran, Detailed chemical kinetic reaction mechanisms for primary reference fuels for diesel cetane number and spark-ignition octane number, *Proc. Combust. Inst.* 33 (2011) 185-192.
- [56] C.K. Westbrook, C.V. Naik, O. Herbinet, W.J. Pitz, M. Mehl, S.M. Sarathy, H.J. Curran, Detailed chemical kinetic reaction mechanisms for soy and rapeseed biodiesel fuels, *Combust. Flame* 158 (2011) 742-755.
- [57] C.K. Westbrook, W.J. Pitz, S.M. Sarathy, M. Mehl, Detailed chemical kinetic modeling of the effects of C=C double bonds on the ignition of biodiesel fuels, *Proc. Combust. Inst.* 34 (2013) 3049-3056.

LIST OF FIGURE CAPTIONS

Figure 1 Molecular structure of the two dominant components of the considered Alcohol-to-Jet Synthetic Paraffinic Kerosene (AtJ-SPK).

Figure 2 Relation between laminar burning velocity (S_u), cone angle (α), and flow velocity (v_u) of a laminar premixed conical flame.

Figure 3 Measurement of ignition delay times: Typical pressure profile with post-shock compression, radially measured excited CH and OH radicals (CH(A) / OH(A)) as well as axially measured CH(A) emission profiles. Here, the emission is decompressed to the input signal of the logarithmic amplifier.

Figure 4 Results of the measured laminar burning velocities (top) and mass burning rate (bottom) of fuel/air mixtures for AtJ-SPK (Alcohol-to-Jet Synthetic Paraffinic Kerosene) in comparison with experimental data of Jet A-1 [11,12] and iso-octane [48] measured at the same experimental conditions.

Figure 5 Results of the measured (symbols) laminar burning velocities for AtJ-SPK (Alcohol-to-Jet Synthetic Paraffinic Kerosene) and iso-octane [48], each in mixture with air at $T = 473$ K in comparison with calculated flame speeds (curves) using the new LLNL mechanism (present work).

Figure 6 Evaluation of the accuracy of the mechanism using the error function value and the average absolute deviation as described by Olm et al. [52].

Figure 7 Sensitivity analysis of laminar flame speed of AtJ-SPK at fuel-air equivalence ratio $\phi = 1.0$.

Figure 8 Comparison between measured (symbols) and calculated (curves) ignition delay times (τ_{ign}) of AtJ-SPK in air at stoichiometric and rich fuel-air ratios with a dilution of N_2 of 1:2. Calculations were performed using the LLNL reaction model developed within the present work. For comparison, measurements of Jet A-1 [11,12] are shown. Error bars shown as example at each ϕ value indicate a variation of the predicted ignition delay time for $p = p$ ($t/s > 0$) $\pm 20\%$ at different initial temperatures.

Figure 9 Plot showing the important reaction pathways in oxidation of Gevo-AtJ surrogate fuel. Flux analysis conducted at 50% conversion of iso-dodecane with initial pressure, temperature and equivalence ratio of 16 bar, 1100 K and $\phi = 2$.

Figure 10 Plots showing the consumption of parent fuels (iso-dodecane: XC12, iso-cetane: HMN), the evolution of different intermediates and formation of carbon oxides.

Figure 11 Brute force sensitivity analyses of ignition delay times (τ_{ign}) for stoichiometric high-pressure ($p = 16$ bar) fuel-air mixtures at $T = 900$ K (top) and $T = 1300$ K (bottom); S_i – sensitivity coefficient for reaction “ i ”, d – dilution, f – factor for perturbation of the reaction rates in mechanism.

Figure 12 Computed ignition delay times (lines) for stoichiometric fuel-air mixtures at $p = 13.6$ bar and $\phi = 1.0$ for iso-cetane (2,2,4,4,6,8,8-heptamethyl nonane, $\text{i-C}_{16}\text{H}_{34}$), iso-dodecane (2,2,4,6,6-pentamethyl heptane, $\text{i-C}_{12}\text{H}_{26}$), iso-octane (2,2,4-trimethyl pentane, $\text{i-C}_8\text{H}_{18}$), iso-heptane (2,2,3-trimethyl butane, $\text{i-C}_7\text{H}_{16}$), and n-heptane ($\text{n-C}_7\text{H}_{16}$), using the LLNL detailed kinetic mechanism. The shown experimental data (dots) of AtJ-SPK (present work) and iso-octane [11] were measured at $p = 16$ bar, corresponding to a deviation of $\pm 15\%$ compared to $p = 13.6$ bar.